



1 **Transport of Asian trace gases via eddy shedding from the Asian summer monsoon**
2 **anticyclone and associated impacts on ozone heating rates**

3 Suvarna Fadnavis¹, Chaitri Roy¹, Rajib Chattopadhyay¹, Christopher E. Sioris², Alexandru
4 Rap³, Rolf Müller⁴, K. Ravi Kumar⁵ and Raghavan Krishnan¹

5 ¹Indian Institute of Tropical Meteorology, Pune, India

6 ²Environment and Climate Change, Toronto, Canada

7 ³School of Earth and Environment, University of Leeds, Leeds, United Kingdom

8 ⁴Forschungszentrum Jülich GmbH, IEK-7, Jülich, Germany

9 ⁵King Abdullah University of Science and Technology, Thuwal, Saudi Arabia

10 *Email of corresponding author: suvarna@tropmet.res.in

11 **Abstract:**

12 The highly vibrant Asian Summer Monsoon (ASM) anticyclone plays an important role in
13 efficient transport of Asian tropospheric air masses to the extratropical upper troposphere and
14 lower stratosphere (UTLS). In this paper, we demonstrate long-range transport of Asian trace
15 gases via eddy shedding events using MIPAS (Michelson Interferometer for Passive
16 Atmospheric Sounding) satellite observations, ERA-Interim re-analysis data and the
17 ECHAM5–HAMMOZ global chemistry–climate model. Model simulations and observations
18 consistently show that the Asian boundary layer trace gases are lifted to UTLS altitudes in the
19 monsoon anticyclone and are further transported horizontally eastward and westward by
20 eddies detached from the anticyclone. We present an event of eddy shedding during 1-8 July
21 2003 and discuss a 1995-2016 climatology of eddy shedding events. Our analysis indicates



22 that eddies detached from the anticyclone are instrumental in distributing the Asian trace gases
23 away from the Asian region to the West-Pacific (20°-30° N; 120°-150° E) and West-Africa
24 (20°-30° N, 0°-30° E). Over the last two decades, the estimated frequency of eddy shedding is
25 ~68 % towards West-Africa and ~25 % towards the West-Pacific.

26 Model sensitivity experiments for a 10 % reduction in Asian emissions of non-methane
27 volatile organic compounds (NMVOCs) and nitrogen oxides (NO_x) were performed with
28 ECHAM5-HAMMOZ to understand the impact of Asian emissions on the UTLS. The model
29 simulations show that transport of Asian emissions due to eddy shedding significantly affects
30 the chemical composition of the upper troposphere (~100-400 hPa) and lower stratosphere
31 (~100-80 hPa) over West-Africa and the West-Pacific. The 10 % reduction of NMVOCs and
32 NO_x Asian emissions leads to decreases in peroxyacetyl nitrate (PAN) (2-10 % near 200-80
33 hPa), ozone (1-4.5 % near ~150 hPa) and ozone heating rates (0.001-0.004 K·day⁻¹ near 300-
34 150 hPa) in the upper troposphere over West-Africa and the West-Pacific.

35 Key Words: Asian summer monsoon anticyclone; Eddy shedding from the monsoon
36 anticyclone, Transport of Asian trace gases, Ozone heating rates; ECHAM5-HAMMOZ
37 model.

38

39

40

41



42 1. Introduction

43 Rapid industrialization, traffic growth, and urbanization resulted in significant increases in the
44 concentrations of tropospheric trace gases, such as carbon dioxide (CO₂), carbon monoxide
45 (CO) and methane (CH₄) over Asia. There is global concern about rising levels of these trace
46 gases (due to their global warming potential) as they are projected to increase further over the
47 coming years despite efforts to implement several mitigation strategies (Ohara et al., 2007). In
48 situ observations, satellite measurements, trajectory analysis and model simulations show long
49 range transport of Asian trace gases to remote locations (e.g. North America, Europe) (Liang
50 et al., 2004). The transported trace gases change the radiative balance, dynamics and chemical
51 composition at the respective locations (Vogel et al., 2016). Satellite observations show
52 increasing trends in several tropospheric Asian trace gases over the last decade, e.g. ozone at
53 ~1-3 % year⁻¹ (Verstraeten et al., 2015), CO at 3% year⁻¹ (Strode and Pawson, 2013), NO_x at
54 ~3.8 -7.3 % year⁻¹ (Schneider and van der A, 2012; Ghude et al., 2013). Biomass burning is
55 another major contributor to the observed growth in these trace gases (van der Werf et al.,
56 2006). Peroxyacetyl nitrate (PAN), a powerful pollutant formed in biomass burning plumes
57 (Wayne, 2000), is a secondary pollutant produced through the oxidation of hydrocarbons
58 released from anthropogenic and biogenic sources. It is a reservoir of reactive nitrogen and
59 plays a fundamental role in the global ozone budget (Tereszchuk et al., 2013; Payne et al.,
60 2017). PAN can also be formed in the upper troposphere through the production of NO_x from
61 lightning (Zhao et al., 2009). Simulations of the Model of Ozone and Related Tracers
62 (MOZART) show an increase of 20-30 % of PAN concentrations in the upper troposphere
63 and lower stratosphere (UTLS) over the Asian summer monsoon (ASM) region produced from



64 lightning (Tie et al., 2002). While in the lower troposphere, PAN has a short lifetime (a few
65 hours), in the UTLS it has a longer lifetime (3-5 months), and can therefore act as a reservoir
66 and carrier of NO_x (Tereszchuk et al., 2013). Recent satellite observations show an increasing
67 trend in PAN ($\sim 0.1 \pm 0.05$ to 2.7 ± 0.8 ppt year⁻¹) in the UTLS over Asia (Fadnavis et al.,
68 2014).

69 Monsoon convection plays an important role in lofting of boundary layer Asian air masses to
70 the UTLS (e.g., Randel et al., 2010; Fadnavis et al., 2015; Santee et al., 2017). The uplifted air
71 masses become confined into the anticyclone enclosed by jets (westerly and easterly jets to the
72 north and south, respectively), which act as a strong transport-barrier and restrict isentropic
73 mixing into the extra-tropical lower stratosphere or the equatorial tropics (Ploeger et al., 2015;
74 Ploeger et al., 2017). Confinements of high amounts of trace gases, including ozone precursors
75 (e.g., hydrogen cyanide (HCN), CO, hydrochloric acid (HCl), NO_x and PAN), and low ozone
76 in the anticyclone are evident in satellite and aircraft observations, (Randel et al., 2010; Vogel
77 et al., 2014; Fadnavis et al., 2015; Ungermann et al., 2016; Santee et al., 2017). The observed
78 ozone minimum in spite of high amounts of its precursors in the anticyclone is still an open
79 question. The trace gases partially enter the lower stratosphere and affect the UTLS chemical
80 composition (Randel et al., 2010; Fadnavis et al., 2015, 2016; Garny and Randel, 2016), with
81 associated radiative forcing impacts (Riese et al., 2012). Cross-tropopause transport associated
82 with the Asian monsoon is evident in a number of species, including aerosols, hydrogen
83 cyanide (HCN) and PAN (Randel et al. 2010; Fadnavis et al. 2014, 2015; Bourassa et al.,
84 2012).



85 The ASM anticyclone is highly dynamic in nature (e.g., Hsu and Plumb, 2000; Popovic and
86 Plumb, 2001; Vogel et al., 2016). On the sub-seasonal scale, it shows variation in strength and
87 location (Garny and Randel, 2016). It frequently sheds eddies and on occasions, it splits into
88 two anticyclones, namely the Tibetan and Iranian anticyclones (Zhang et al., 2002; Nützel et
89 al., 2016). An eddy detached from the anticyclone carries Asian air masses (trace gases) away
90 from the ASM region. There are scattered studies indicating eddy shedding to the west
91 (Popovic and Plumb, 2001) and east (Ungermann et al., 2016; Vogel et al., 2014) of the
92 anticyclone. An eddy shedding event causes irreversible mixing in the surrounding air
93 changing the chemical composition and radiative balance of that region (Garny and Randel,
94 2016). Here, we analyze in detail transport of Asian trace gases via eddies, subsequent mixing
95 into the extra-tropics and radiative impact of eddy shedding events on decadal scales. In this
96 paper, we ask the following questions: (1) how frequent were eddy shedding events during the
97 last two decades? (2) Which regions are the most affected? (3) Does the transport of Asian
98 trace gases arising from eddy shedding affect UTLS ozone concentrations and heating rates at
99 remote locations?

100 To address these questions, we first consider an eddy shedding event demonstrating eastward
101 and westward shedding from the ASM anticyclone during 1-8 July 2003. This year was chosen
102 since the monsoon season was quite normal (i.e., no evidence of El Niño or Indian Ocean
103 dipole phenomenon influencing the monsoon circulation). We then present a climatology of
104 eddy shedding events and lead-lag relations of eddies with the anticyclone. We also evaluate
105 the impact of increasing Asian emissions of NO_x and NMVOCs on ozone and PAN during the
106 eddy shedding event, using model sensitivity simulations. Finally, we estimate the associated



107 changes in ozone heating rates in the UTLS due to Asian trace gases transported via eddy
108 shedding events.

109 **2. Experimental set-up and satellite observations**

110 **2.1 Satellite observations**

111 The MIPAS (Michelson Interferometer for Passive Atmospheric Sounding) instrument was
112 launched in March 2002 into a polar orbit of 800 km altitude. Its orbital period is about 100
113 min. MIPAS-E provided continual limb emission measurements in the mid-infrared over the
114 range 685– 2410 cm^{-1} (14.6–4.15 μm) until December 2004 (Fischer et al., 2008). From
115 January 2005 through April 2012, MIPAS-E was operated with a reduced spectral resolution,
116 and a vertical resolution of 3 km of in the UTLS region. MIPAS monitored many atmospheric
117 trace constituents including CO, PAN, and O₃. The details of the general retrieval method and
118 setup, error estimates and use of averaging kernel and visibility flag are documented by von
119 Clarmann et al. (2009). Here, we analyze the MIPAS observed CO, PAN, and O₃ data during
120 1-8 July 2003.

121 To account for the comparatively low, and altitude-dependent vertical resolution of MIPAS,
122 the model data were convolved with the MIPAS averaging kernel to be directly comparable to
123 MIPAS measurements of CO, PAN, and ozone. MIPAS vertical resolution for CO, O₃ and
124 PAN in the UTLS is 5, 3.5 and 5 km, respectively. The data are contoured and gridded at 15°
125 latitude and 10° longitude resolution. In the process, the data quality specifications as
126 documented at <http://share.lsfdf.kit.edu/imk/asf/sat/mipas-export/Documentation/> were



127 employed, namely: only data with a visibility flag equal to 1 and a diagonal value of averaging
128 kernel greater than 0.03 were used for ozone and PAN, while 0.008 was used for CO.

129 **2.2 Experimental set-up**

130 We employ the ECHAM5-HAMMOZ (Roeckner et al., 2003) aerosol-chemistry-climate
131 model to understand re-distribution of Asian trace gases via eddy shedding from the
132 anticyclone. ECHAM5-HAMMOZ comprises of the general circulation model ECHAM5
133 (Roeckner et al., 2003), the tropospheric chemistry module MOZ (Horowitz et al., 2003), and
134 the aerosol module, Hamburg Aerosol Model (HAM) (Stier et al., 2005). The chemistry of
135 ozone, VOCs, NO_x, and other gas-phase species is based on the MOZART-2 chemical scheme
136 (Horowitz et al., 2003). It includes O_x-NO_x-hydrocarbons with 63 tracers and 168 reactions.
137 The details of the parameterizations and emissions used in the model as well as a validation of
138 the results are described by Fadnavis et al. (2013, 2014, 2015) and Pozzoli et al. (2011).

139 The model simulations were performed at the T42 spectral resolution corresponding to about
140 2.8° × 2.8° in the horizontal dimension and 31 vertical hybrid σ -p levels from the surface up to
141 10 hPa. Here, we note that our base year for aerosol and trace gas emissions is 2000. We
142 performed two simulations: (i) a control experiment (CTRL), and (ii) a sensitivity experiment
143 (Asia10), where emissions of both NO_x and NMVOCs were simultaneously reduced by 10 %
144 over Asia (10° S–50° N, 60–130° E). Both simulations were performed for the year 2003
145 driven by European Centre for Medium-Range Weather Forecasts operational analyses
146 (Integrated Forecast System (IFS) cycle-32r2) meteorological fields (available every six
147 hours) (Uppala et al., 2005). All simulations include lightning NO_x and the subsequent PAN



148 production. Since the lightning parameterization is the same in the CTRL and sensitivity
149 simulations, its impact may be negligible. However, there may be an indirect impact of
150 changed emissions on lightning and thus on NO_x or PAN production. The model simulations
151 used here are the same as those used by Fadnavis et al. (2015).

152 The climatology of ozone mass mixing ratio, winds and Potential Vorticity (PV) are obtained
153 from ERA-Interim reanalysis data for the period 1995-2016. The anomalies are obtained from
154 difference between daily mean values of July 2003 and daily climatology. Power spectral
155 analysis and lag/lead correlations have been carried out on PV data for the period 1995-2016
156 to show climatological features.

157 Instantaneous ozone heating rates are calculated using the Edwards and Slingo (1996)
158 radiative transfer model. We used the off-line version of the model, with six shortwave and
159 nine longwave bands, and a delta-Eddington 2-stream scattering solver at all wavelengths, in a
160 set-up similar to other recent studies (Rap et al., 2015, Roy et al., 2017).

161 **3. Results**

162 **3.1 A typical case study of eddy shedding from the monsoon anticyclone**

163 The dynamics of the monsoon anticyclone is better portrayed at the 370 K potential
164 temperature surface and the monsoon anticyclone is obvious as an area of low PV values (PV <
165 2 PVU, 1 PVU = 10⁻⁶ K m² kg⁻¹ s⁻¹) (indicating tropospheric air-mass) at this surface (Garny
166 and Randel, 2016). Eddies are identified as air with low PV emanating from the monsoon
167 anticyclone (Popovic and Plumb, 2001; Vogel et al., 2014). Past studies have shown that



168 during the monsoon season (June to September), the bulk of the low PV air at the isentropic
169 level of 370 K, is confined between about 20–35° N and 20–120° E indicating the spatial
170 extent of the anticyclone (Popovic and Plumb, 2001; Vogel et al., 2014; Garny and Randel,
171 2016). A pocket of low PV air-mass detached from the boundary of the anticyclone (outside
172 the anticyclone, 20–35° N and 20–120° E) is considered as an eddy. **Figure 1a-h** shows the
173 distribution of PV at 370 K during 1-8 July 2003. It can be seen that during this period the
174 anticyclone was wobbling and shed eddies eastward and westward over West-Africa (20-30°
175 N, 0-30° E) and the West-Pacific (20-30° N; 120-150° E). Initially, during 2-5 July 2003, the
176 ASM anticyclone shed an eddy westward over West-Africa. The eddy moved further west
177 with the progression of time. Later during 4-8 July 2003, eddy shedding occurred to the east of
178 the anticyclone, over the West-Pacific and the air detached from the anticyclone moved further
179 eastward with time. The longitude-pressure section of PV shows that the eddy protrudes down
180 to 400 hPa (not shown).

181 Previous studies have shown that eddy shedding events are associated with Rossby wave
182 breaking (RWB) (Hsu and Plumb, 2000; Popovic and Plumb, 2001; Fadnavis and
183 Chattopadhyay, 2017). The RWB is manifested as a rapid and large-scale irreversible
184 overturning of PV contours on the 350K isentropic surface. It is accompanied with a cyclonic
185 circulation at 200 hPa (Strong and Magnusdottir, 2008; Fadnavis and Chattopadhyay, 2017).
186 **Figure 2a-h** shows the distribution of PV at the 350K surface and the circulation at 200 hPa
187 during 1-8 July 2003. It can be seen that, during 1-8 July 2003, three RWB events occurred:
188 one near 30° E (referred as RWB-1), one near 70° E (referred as RWB-2) and another one



189 near 120°E (referred to as RWB-3). Since RWB-3 was outside the region of the ASM
190 anticyclone (over the West-Pacific ~150-170° E) it did not play a role in the eddy shedding
191 event of 1-8 July. If we track the location of these RWB events (indicated by the black and red
192 arrows), one can see that, with the progression of time, the RWB feature moved eastward. The
193 eastward migration of RWB is linked to its movement along the subtropical westerly jet
194 (Fadnavis and Chattopadhyay, 2017). Initially during 1-5 July RWB-1 was strong ($PV > 2$
195 PVU) while RWB-2 ($PV < 2$ PVU) was weak. During this period the southward and westward
196 moving RWB-1 leads to eddy shedding over West Africa. Later, during 4-8 July, RWB-2
197 strengthened while RWB-1 weakened and disappeared. The southward and eastward moving
198 RWB-2 was responsible for the eddy shedding event near the Western Pacific (see **Fig. 2d-h**).

199 **3.2. Climatology of eddy shedding from the monsoon anticyclone**

200 A power spectrum analysis has been performed on the PV data (averaged for 300-100 hPa)
201 during 1995-2016 for West-Africa (20-30° N, 0-30° E) and the West-Pacific (20-30° N, 140-
202 150° E). **Figure 3a-b** shows the distribution of power spectral variance over these two regions.
203 The variance is significant at 99 % for 3-5 days and 12-15 days for both the regions indicating
204 that the eddy shedding activity is dominated in the range of synoptic frequency (~10 days).
205 Popovic and Plumb (2001) also indicated a typical duration of an eddy shedding event of ~4-8
206 days. We compute the frequency of eddy shedding days ($PV < 1$ PVU) occurring over West-
207 Africa and the Western Pacific. The ERA-Interim data for the last two decades show that eddy
208 shedding is quite frequent over west-Africa ~68 % and the West-Pacific ~25 %. The lag-lead
209 correlation of PV (averaged for 200-100 hPa) for the centre region of the anticyclone (85-90°



210 E, 28-30° N) with PV averaged over the West-Pacific shows a maximum positive lead
211 correlation at 3-4 days (**Fig. 3c**). Similarly, PV over West-Africa shows a maximum positive
212 lead correlation for 5-6 days with the PV averaged over the monsoon anticyclone (**Fig. 3d**).
213 This indicates that the transport of the eddies from the anticyclone (source region) has a
214 typical duration of three to four days over the West Pacific and five to six days over West
215 Africa. This transport time is the timescale over which the trace gases are moved to remote
216 locations from the ASM anticyclone.

217 **3.3. Long range transport of trace gases**

218 **3.3.1 Horizontal transport of ozone, CO and PAN via eddies**

219 Biomass burning over south-east Asia and East Asia produces large amounts of CO, NO_x,
220 VOCs, PAN, ozone and aerosols (e.g., Streets et al., 2003, Fadnavis et al., 2014). The
221 monsoon convection over the Bay of Bengal, southern slopes of Himalaya and South China
222 Sea (see **Fig. S1**) lifts up these species into the anticyclone where they may get dispersed in
223 the UTLS by the vibrant anticyclone and its associated eddies. **Figure 4a-h** shows the
224 distribution of ozone during 1-8 July 2003 (MIPAS O₃ is binned for 2 days and simulated O₃
225 is plotted for alternate days) in the anticyclone at 16 km (~100 hPa). Ozone concentrations
226 from MIPAS satellite measurements and model simulations (CTRL) are plotted at 16 km and
227 from ERA-Interim reanalysis at 100 hPa. For comparison, we have interpolated the model data
228 to the MIPAS altitude grid and smoothed with the averaging kernel. The ASM anticyclone is
229 marked by minimum ozone although its precursors (e.g. CO, NO_x and CH₄) show maxima
230 (Randel et al., 2010; Roy et al., 2017). The spatial pattern of low ozone amounts in the



231 anticyclone and the associated eddies is evident in all of the data sets during 1-8 July 2003.
232 During 1-5 July, ozone concentrations in the eddy over West-Africa are ~60-200 ppb in
233 MIPAS, ~60-100 ppb in ERA-Interim and 80-150 ppb in the model simulations. During 4-8
234 July, the eddy over the west Pacific shows ozone amounts of ~80-200 ppb in MIPAS, ~80-120
235 ppb in ERA-Interim and ~150-200 ppb in the model simulations. In general, MIPAS
236 measurements and simulated ozone amounts shows reasonable agreement, while ozone
237 amounts in ERA-Interim are lower by 30-80 ppb than both MIPAS measurements and the
238 model simulations.

239 **Figure 5a-h** shows the distribution of CO from MIPAS observations and model simulations
240 during 1-8 July 2003 (MIPAS CO is binned for 2 days and simulated CO is plotted for
241 alternate days). The confinement of high concentrations of CO in the anticyclone and in eddies
242 is seen in both MIPAS observations and model simulations. During 1-5 July, eddies over west-
243 Africa and west-Pacific show CO volume mixing ratios of ~65-85 ppb in MIPAS, and ~70-90
244 ppb in the model simulations.

245 **Figure 6a-h** shows the distribution of PAN from MIPAS measurements and the model
246 simulation (CTRL) at 16km during 1-8 July 2003 (MIPAS PAN mixing ratios are binned for
247 2 days and simulated PAN is plotted for alternate days). A confinement of high amounts of
248 PAN in the anticyclone and the associated eddies is seen both in the MIPAS measurements
249 and the model simulations. During 1-5 July, MIPAS observed PAN amounts are ~120-230 ppt
250 in eddies over west-Africa, while the model simulation shows ~180-240 ppt of PAN at the



251 same location. The eddy over the west-Pacific shows PAN amounts of ~120-230 ppt in the
252 MIPAS measurements and 160-230 ppt in the model simulations.

253 There are minor differences in ozone, CO and PAN amounts from model simulation, satellite
254 observations and ozone from ERA-Interim. These differences may be due to a number of
255 reasons e.g. different grid sizes of MIPAS ($10^{\circ}\times 15^{\circ}$), ERA-Interim ($0.75^{\circ}\times 0.75^{\circ}$) and model
256 data ($2.8^{\circ}\times 2.8^{\circ}$), binning of MIPAS data for two days to accommodate better special
257 coverage, uncertainties in the model emission inventory, and retrieval errors in the satellite
258 data.

259 3.3.2 Vertical distribution of CO, PAN and ozone

260 Further, we show the vertical distribution of CO and PAN as an indication of the Asian
261 biomass burning emissions. **Figure 7** shows longitude-pressure cross-sections (averaged for
262 20° - 40° N) of CO and PAN from the CTRL simulation, with wind vectors depicting
263 circulation patterns. It shows during 1-5 July 2003 a plume of CO/PAN uplifted from the
264 Asian region (80° - 120° E) moving further upward into the UTLS. The location of the plume
265 coincides with the region of convective transport (**Fig. S1**). In the upper troposphere (~120
266 hPa) westward horizontal transport of CO/PAN towards West-Africa is obvious as a result of
267 eddy shedding during the respective days. In particular, during 2-4 July high amounts of
268 CO/PAN are observed near 0° - 30° E at 100 hPa (**Fig. 7a-b** and **7e-f**). On 2 July there is some
269 PAN transport over west-Pacific. During 4-8 July 2003, eddy shedding occurs to the east of
270 the anticyclone over the West-Pacific (120° - 150° E) (see Figure 1e-f). East-ward horizontal
271 transport of CO/PAN in the regions of eddy shedding is evident in **Fig.7c-d** and **7g-h**. The



272 Asian trace gases then disperse downward deep into the troposphere (~500 hPa over the West
273 Pacific and ~200 hPa over West-Africa) and are partially lifted into the lower stratosphere.

274 The vertical distribution of ozone shows low ozone amounts extending from convective
275 regions of the Bay of Bengal (80-95° E) and the South China Sea (~120° E) upward in the
276 upper troposphere (**Fig.S2**). This is due to low ozone amounts in marine air masses over Asia
277 during the monsoon season (Zhao et al., 2009). This feature is not as clear as seen in the
278 vertical distribution of CO and PAN, since a number of factors are influencing ozone
279 production and loss processes at different altitudes in the troposphere and lower stratosphere
280 (e.g. lightning in the upper troposphere).

281 **3.4 Influence of Asian emissions on extra-tropical UTLS**

282 In this section, we investigate the influence of Asian anthropogenic emissions of
283 NMVOCs and NO_x on the distribution of PAN and ozone in the tropical/extra-tropical UTLS
284 from sensitivity experiments. **Figure 8a-d** shows anomalies of PAN (Asia10-CTRL) at 16km
285 during 1-8 July 2003 (plotted on alternate days). The negative anomalies in PAN are seen
286 confined to the region of the anticyclone and the associated eddies (1-5 July over West-Africa
287 and 4-8 July over West-Pacific). These anomalies portray the response of Asian boundary
288 layer emissions (NMVOCs and NO_x) on the upper level anticyclone and the associated eddies.
289 A number of studies (Randel et al., 2010; Fadnavis et al., 2013; 2015; Vogel et al., 2014) have
290 shown lifting of Asian emissions to the UTLS by the monsoon convection and its confinement
291 in the anticyclone. Decrease in Asian emissions (NMVOCs and NO_x) by 10 % decreases PAN



292 amounts by ~5-23 % in the ASM anticyclone and the associated eddies over West-Africa and
293 the West-Pacific.

294 Further, we analyze the vertical distribution of anomalies of PAN and ozone. Figure 8e-h
295 shows longitude-pressure sections of anomalies of PAN. It shows negative anomalies (in
296 response to reduced Asian emissions) along the transport pathways (**Fig. S1**), i.e., from the
297 boundary layer of the Asian region (80°-120° E) into the upper troposphere and
298 westward/eastward transport from the anticyclone owing to eddy shedding. These anomalies
299 extending above the tropopause indicate cross-tropopause transport. Our simulations show that
300 a 10 % reduction in Asian emissions of both NMVOCs and NO_x, results in a decrease in the
301 amount of PAN by ~2-10 % over North-West Africa during 1-5 July and over the Western
302 Pacific during 4-8 July 2003.

303 The vertical distribution of ozone anomalies show negative values (-1 to -4.5 %) in the
304 troposphere extending from the surface up to 180 hPa along the transport pathways (80°-110°
305 E). Near the tropopause ozone anomalies are positive, varying between 1 to 8 % (**Fig.8i-l**).
306 During the monsoon season, marine air masses containing low amounts of ozone prevail over
307 the Asian land mass. The monsoon air mass gathers Asian boundary layer ozone precursors
308 (and the other trace gases) and is uplifted to the UTLS by the monsoon circulation. It should
309 be noted that a decrease in emissions of NO_x and NMVOCs in the Asia10 simulations
310 produces lower ozone amounts in the troposphere than CTRL. Therefore, in the regions of
311 eddy shedding, negative anomalies near 200-300 hPa indicate transport of monsoon air (via
312 eddies) towards West-Africa during 1-5 July and to the West-Pacific during 4-8 July. Also,



313 there may be ozone production in the troposphere from its precursors carried by the monsoon
314 circulation. PAN transported by eddies in the troposphere over West-Africa and the West
315 Pacific will release NO_x and contributes to tropospheric ozone production (**Fig. 7e-h** and **Fig.**
316 **8e-h**). The increase in lower stratospheric ozone concentrations near the tropopause (Fig. 8i-l),
317 in response to the 10 % reduction of Asian NO_x and NMVOCs emissions, may be due to the
318 inverse relation between ozone amounts and its precursors in the monsoon anticyclone
319 (Randel et al., 2010) and other factors such as changes in dynamics due to emission change.
320 Ozone changes near the tropopause have been shown to have a large impact on the Earth's
321 radiative balance (Riese et al., 2012).

322 **3.5 Influence of Asian emission of trace gases on ozone heating rates**

323 Ozone is a dominant contributor to radiative heating in the tropical lower stratosphere,
324 impacting the local heating budget and non-local forcing of the troposphere below (Gilford
325 and Solomon, 2017). We estimate changes in ozone heating rates caused by a 10 % decrease
326 in Asian NMVOCs and NO_x emissions. **Figure 9a-d**, showing anomalies of ozone heating
327 rates on 1-8 July (plotted on alternate days), indicates a reduction in ozone heating rates in
328 response to a decrease in Asian NMVOCs and NO_x emissions, coincident with the region of
329 convective transport (**Fig. S1**). In the upper troposphere (300-180 hPa), the negative anomalies
330 in ozone heating rates vary between -0.001 and $-0.0045 \text{ K}\cdot\text{day}^{-1}$. Interestingly, reduced Asian
331 emissions (NMVOCs and NO_x), leads to a reduction in ozone, which leads to a reduction in
332 ozone heating rates (-0.001 to $-0.003 \text{ K}\cdot\text{day}^{-1}$) in the region of eddy shedding over West-
333 Africa (1-5 July) and the West-Pacific (4-8 July). The ozone poor Asian air mass trapped



334 within eddies has reduced the heating over West-Africa and the West-Pacific. Influence of
335 Asian NO_x emissions on ozone heating rates (mean for June-September $\sim 0.0001 - 0.0012$
336 $\text{K}\cdot\text{day}^{-1}$ for 38 % increase over India) in the upper troposphere (300-200 hPa) have been
337 reported in the past (Roy et al., 2017). Near the tropopause, ozone heating rates are positive
338 $0.001 - 0.005 \text{ K}\cdot\text{day}^{-1}$, which is due to positive anomalies of ozone near the tropopause (**Fig.**
339 **8i-1**). The ECMWF dataset for 44 years (1958-2001) shows an inter-annual amplitude of the
340 ozone heating rate $\pm 0.00025 \text{ K}\cdot\text{day}^{-1}$ near the tropopause over $30^\circ \text{S}-30^\circ \text{N}$ (Wang et al. 2008).

341 **4. Summary and Discussion**

342 In this study we show evidence of eddy shedding from the ASM anticyclone to both its eastern
343 and western edge, during 1-8 July 2003 based on MIPAS satellite observations and ERA
344 Interim re-analysis data as well as the associated transport patterns of trace gases from the
345 ASM region to remote regions. The transport diagnostic based on ERA-Interim data shows
346 that eddy shedding events are associated with RWB in the subtropical westerly jet. The RWB
347 feature moves eastward in the subtropical westerly jet. Initially, during 1-5 July 2003, RWB
348 occurs in the western part of the anticyclone and then sheds over West-Africa ($20^\circ-30^\circ \text{N}$, $0^\circ-$
349 30°E). Later, during 5-8 July 2003, RWB moves to the eastern part of the anticyclone and
350 sheds an eddy over the West-Pacific ($20^\circ-30^\circ \text{N}$; $120^\circ-150^\circ \text{E}$). Analysis of ERA-Interim PV
351 data for the last two decades (1995-2016) shows that the frequency of eddy shedding from the
352 ASM anticyclone over West-Africa is $\sim 68\%$ and $\sim 25\%$ over the West-Pacific. PV (300-100
353 hPa) at the centre of the anticyclone ($85^\circ-90^\circ \text{E}$, $28^\circ-30^\circ \text{N}$) shows maximum correlation with
354 PV over West-Africa 3-4 days later and 5-6 days later in the West-Pacific. It indicates that the



355 anticyclone sheds eddies with transport duration of typically three to four days to West Africa
356 and five-six days to the Western Pacific.

357 We employ the chemistry climate model ECHAM5-HAMMOZ to investigate transport of
358 Asian boundary layer trace gases (CO, ozone and PAN) into the monsoon anticyclone and the
359 associated eddies. The model simulations show that Asian trace gases transported into the
360 monsoon anticyclone are further carried away horizontally towards West-Africa and the West-
361 Pacific by eddies which detach from the anticyclone. These eddies protrude down to ~200 hPa
362 over West-Africa and ~500 hPa over the West Pacific. They re-distribute Asian trace gases
363 downward into the troposphere over these regions. Moreover, part of this air-mass is also
364 transported upward into the lower stratosphere. A higher frequency of eddy shedding over
365 West-Africa (68 %) during last two decades indicates a greater influence of Asian trace gases
366 on the UTLS over West-Africa than the West-Pacific over last two decades (1995-2016).

367 We evaluate the impact of Asian NO_x and NMVOCs emissions on ozone and PAN in
368 the regions of the ASM anticyclone and the associated eddies. The model sensitivity
369 simulations for a 10 % reduction in Asian emissions of NMVOCs and NO_x indicate significant
370 reduction (~2-10 %) in the concentration of PAN in the UTLS (300-80 hPa) over West-Africa
371 and the West-Pacific. The vertical distribution of anomalies of PAN shows negative values
372 along the transport pathways, i.e., rising from the Asian region (80°-120° E) into the upper
373 troposphere and both westward and eastward transport towards the region of eddy shedding.
374 Tropospheric ozone (1000-180 hPa) shows a decrease of up to -4.5 % in response to a 10 %
375 decrease in Asian emissions of NMVOCs and NO_x, while positive ozone anomalies (up to 8



376 %) are seen near the tropopause. The reason for the observed ozone minimum (noting that
377 ozone precursors show high amounts) in the anticyclone is still an open question. The satellites
378 and aircraft observations show inverse relation between the amount of ozone and its
379 precursors. The increase in ozone anomalies in the anticyclone in response to a reduction of
380 NO_x and NMVOCs may be a consequence of the observed inverse relation between ozone and
381 its precursors in the anticyclone or it may be due to changes in dynamics in response to
382 emission change, which requires further investigations.

383 Our analysis indicates that transport of Asian trace gases from the anticyclone to West-Africa
384 and the West-Pacific via eddies causes a change in the chemical composition of the UTLS and
385 may therefore impact the radiative balance of the UTLS. We also estimate that a 10 %
386 reduction in Asian NMVOCs and NO_x emissions leads to a decrease of ozone heating rates of
387 0.001 to 0.004 $\text{K}\cdot\text{day}^{-1}$ in the region of transport into the troposphere and an increase of 0.001
388 to 0.005 $\text{K}\cdot\text{day}^{-1}$ near the tropopause and lower stratosphere (180-50 hPa) over Asia (20°-150°
389 E; 20°-40° N). Previous studies show that ozone changes in the lower stratosphere have the
390 largest impact on the ozone radiative forcing (Riese et al., 2012). Interestingly, in the upper
391 troposphere (200-300 hPa) negative anomalies of ozone heating rates ($\sim 0.001\text{-}0.003 \text{ K}\cdot\text{day}^{-1}$)
392 are seen in the region of eddy shedding over West-Africa and the West-Pacific. Thus transport
393 of Asian air masses via eddies eventually alters the heating rates in the UTLS in the regions of
394 eddy shedding and may thus affect radiative forcing and local temperature. However such
395 questions are beyond the scope of this study. It should be noted that there are minor
396 differences in the amounts of ozone, CO and PAN between model simulations and satellite
397 observations (ozone from ERA-Interim). The ozone heating rates estimated from the model



398 simulations will vary accordingly. Notwithstanding, we suggest further scrutiny of long range
399 transport of Asian trace gases via eddies shedding from the anticyclone and its impact on
400 ozone heating rates in the respective regions.

401 **Acknowledgements:** Dr. S. Fadnavis and C. Roy acknowledges with gratitude Prof. Ravi
402 Nanjundiah, Director of IITM, for his encouragement during the course of this study. We are
403 grateful to B. Vogel for helpful discussions. This work was partly funded by the European
404 Community's Seventh Framework Programme (FP7/2007–2013) as part of the StratoClim
405 project (grant agreement no. 603557). We thank the European Centre for Medium-Range
406 Weather Forecasts (ECMWF) for providing meteorological data sets. The authors are also
407 thankful to Dr. Bernd Funke and Dr. Michael Kiefer for their help related to MIPAS data.

408 **References:**

- 409 Bourassa, A. E., Robock, A., Randel, W. J., Deshler, T., Rieger, L. A., Lloyd, N. D.,
410 Llewellyn, E. J. and Degenstein, D. A.: Large volcanic aerosol load in the stratosphere
411 linked to Asian monsoon transport, *Science*, 336(6090), 78–81,
412 doi:10.1126/science.1219371, 2012.
- 413 Edwards, J. M. and Slingo, A.: Studies with a flexible new radiation code. I: Choosing a
414 configuration for a large-scale model, *Q. J. R. Meteorol. Soc.*, 122(531), 689–719,
415 doi:10.1256/smsqj.53106, 1996.
- 416 Fadnavis, S., Semeniuk, K., Pozzoli, L., Schultz, M. G., Ghude, S. D., Das, S. and Kakatkar,
417 R.: Transport of aerosols into the UTLS and their impact on the asian monsoon region
418 as seen in a global model simulation, *Atmos. Chem. Phys.*, 13(17), 8771–8786,
419 doi:10.5194/acp-13-8771-2013, 2013.
- 420 Fadnavis, S., Schultz, M. G., Semeniuk, K., Mahajan, A. S., Pozzoli, L., Sonbawne, S., Ghude,
421 S. D., Kiefer, M. and Eckert, E.: Trends in peroxyacetyl nitrate (PAN) in the upper
422 troposphere and lower stratosphere over southern Asia during the summer monsoon
423 season: Regional impacts, *Atmos. Chem. Phys.*, 14(23), 12725–12743,
424 doi:10.5194/acp-14-12725-2014, 2014.
- 425 Fadnavis, S., Semeniuk, K., Schultz, M. G., Kiefer, M., Mahajan, A., Pozzoli, L. and
426 Sonbawane, S.: Transport pathways of peroxyacetyl nitrate in the upper troposphere
427 and lower stratosphere from different monsoon systems during the summer monsoon
428 season, *Atmos. Chem. Phys.*, 15(20), 11477–11499, doi:10.5194/acp-15-11477-2015,
429 2015.
- 430 Fadnavis, S. and Chattopadhyay, R.: Linkages of subtropical stratospheric intraseasonal
431 intrusions with Indian summer monsoon deficit rainfall, *J. Clim.*, 30(13), 5083–5095,
432 doi:10.1175/JCLI-D-16-0463.1, 2017.
- 433 Fischer, H., Birk, M., Blom, C., Carli, B., Carlotti, M., von Clarmann, T., Delbouille, L.,
434 Dudhia, A., Ehhalt, D., Endemann, M., Flaud, J. M., Gessner, R., Kleinert, A.,
435 Koopman, R., Langen, J., López-Puertas, M., Mosner, P., Nett, H., Oelhaf, H., Perron,
436 G., Remedios, J., Ridolfi, M., Stiller, G. and Zander, R.: MIPAS: An instrument for
437 atmospheric and climate research, *Atmos. Chem. Phys.*, 8(8), 2151–2188,
438 doi:10.5194/acp-8-2151-2008, 2008.
- 439 Garny, H. and Randel, W. J.: Transport pathways from the Asian monsoon anticyclone to the
440 stratosphere, *Atmos. Chem. Phys.*, 16(4), 2703–2718, doi: 10.5194/acp-16-2703-2016,
441 2016.
- 442 Ghude, S. D., Kulkarni, S. H., Jena, C., Pfister, G. G., Beig, G., Fadnavis, S. and van Der, R.
443 J.: Application of satellite observations for identifying regions of dominant sources of



- 444 nitrogen oxides over the indian subcontinent, *J. Geophys. Res. Atmos.*, 118(2), 1075–
445 1089, doi: 10.1029/2012JD017811, 2013.
- 446 Gilford, D. M. and Solomon, S.: Radiative effects of stratospheric seasonal cycles in the
447 tropical upper troposphere and lower stratosphere, *J. Clim.*, 30(8), 2769–2783,
448 doi:10.1175/JCLI-D-16-0633.1, 2017.
- 449 Horowitz, L. W., Walters, S., Mauzerall, D. L., Emmons, L. K., Rasch, P. J., Granier, C., Tie,
450 X., Lamarque, J.-F., Schultz, M. G., Tyndall, G. S., Orlando, J. J. and Brasseur, G. P.:
451 A global simulation of tropospheric ozone and related tracers: Description and
452 evaluation of MOZART, version 2, *J. Geophys. Res. Atmos.*, 108(D24), doi:
453 10.1029/2002JD002853, 2003.
- 454 Hsu, C. J. and Plumb, R. A.: Nonaxisymmetric Thermally Driven Circulations and Upper-
455 Tropospheric Monsoon Dynamics, *J. Atmos. Sci.*, 57(1977), 1255–1276,
456 doi:[https://doi.org/10.1175/1520-0469\(2000\)057<1255:NTDCAU>2.0.CO;2](https://doi.org/10.1175/1520-0469(2000)057<1255:NTDCAU>2.0.CO;2), 2000.
- 457 Liang, Q., Jaeglé, L., Jaffe, D. A., Weiss-Penzias, P., Heckman, A. and Snow, J. A.: Long-
458 range transport of Asian pollution to the northeast Pacific: Seasonal variations and
459 transport pathways of carbon monoxide, *J. Geophys. Res. D Atmos.*, 109(23), 1–16,
460 doi:10.1029/2003JD004402, 2004.
- 461 Nützel, M., Dameris, M., and Garny, H.: Movement, drivers and bimodality of the South Asian
462 High, *Atmos. Chem. Phys.*, 16, 14755–14774, [https://doi.org/10.5194/acp-16-14755-](https://doi.org/10.5194/acp-16-14755-2016)
463 2016, 2016.
- 464 Ohara, T., Akimoto, H., Kurokawa, J., Horii, N., Yamaji, K., Yan, X. and Hayasaka, T.: An
465 Asian emission inventory of anthropogenic emission sources for the period 1980–2020,
466 *Atmos. Chem. Phys.*, 7, 4419–4444, doi:10.5194/acp-7-4419-2007, 2007.
- 467 Payne, V. H., Fischer, E. V., Worden, J. R., Jiang, Z., Zhu, L., Kurosu, T. P. and Kulawik, S.
468 S.: Spatial variability in tropospheric peroxyacetyl nitrate in the tropics from infrared
469 satellite observations in 2005 and 2006, *Atmos. Chem. Phys.*, 17(10), 6341–6351,
470 doi:10.5194/acp-17-6341-2017, 2017.
- 471 Ploeger, F., Gottschling, C., Griessbach, S., Groß, J.-U., Guenther, G., Konopka, P., Müller,
472 R., Riese, M., Stroh, F., Tao, M., Ungermann, J., Vogel, B. and von Hobe, M.: A
473 potential vorticity-based determination of the transport barrier in the Asian summer
474 monsoon anticyclone, *Atmos. Chem. Phys.*, 15(22), 13145–13159, doi:10.5194/acp-
475 15-13145-2015, 2015.
- 476 Ploeger, F., Konopka, P., Walker, K. and Riese, M.: Quantifying trace gases transport from the
477 Asian monsoon anticyclone into the lower stratosphere, *Atmos. Chem. Phys.*, 17(11),
478 7055–7066, doi: 10.5194/acp-17-7055-2017, 2017.
- 479 Popovic, J. M. and Plumb, R. A.: Eddy Shedding from the Upper-Tropospheric Asian



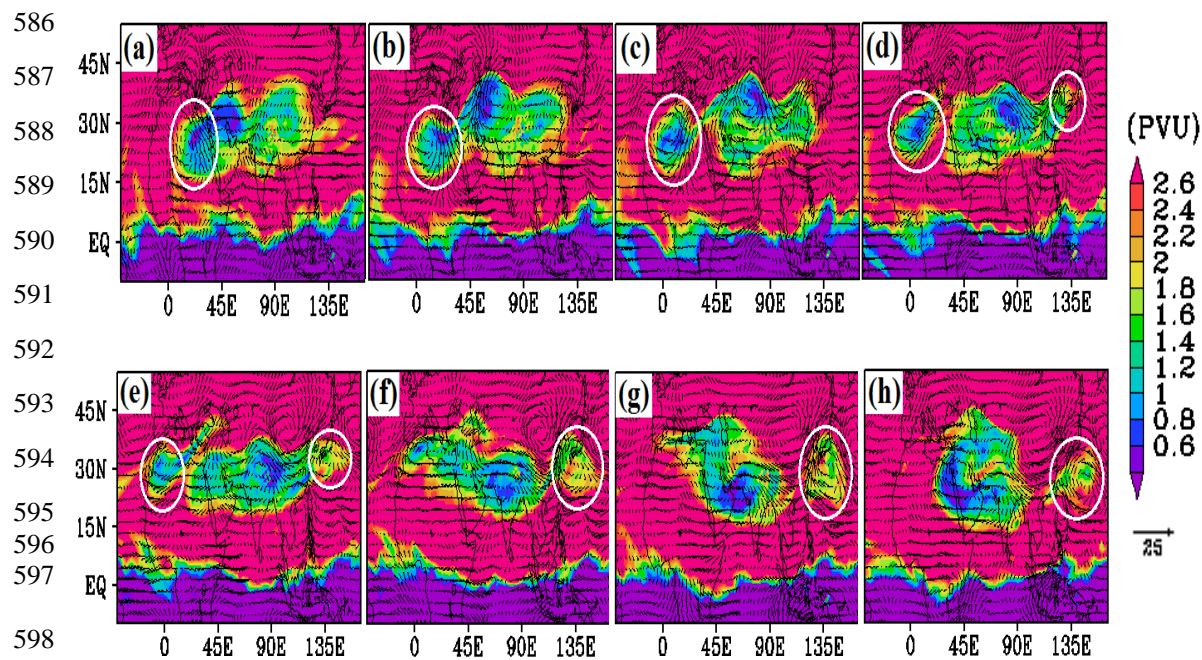
- 480 Monsoon Anticyclone, *J. Atmos. Sci.*, 58(1), 93–104, doi:[https://doi.org/10.1175/1520-0469\(2001\)058<0093:ESFTUT>2.0.CO;2](https://doi.org/10.1175/1520-0469(2001)058<0093:ESFTUT>2.0.CO;2), 2001.
- 482 Pozzoli, L., Janssens-Maenhout, G., Diehl, T., Bey, I., Schultz, M. G., Feichter, J., Vignati, E.
483 and Dentener, F.: Re-analysis of tropospheric sulfate aerosol and ozone for the period
484 1980-2005 using the aerosol-chemistry-climate model ECHAM5-HAMMOZ, *Atmos.*
485 *Chem. Phys.*, 11(18), 9563–9594, doi:10.5194/acp-11-9563-2011, 2011.
- 486 Randel, W. J., Park, M., Emmons, L., Kinnison, D., Bernath, P., Walker, K. A., Boone, C., and
487 Pumphrey, H.: Asian monsoon transport of trace gases to the stratosphere, *Science*,
488 328, 611-613, 10.1126/science.1182274, 2010.
- 489 Rap A., Richards N.A.D.; Forster P.M.; Monks S.; Arnold S.R.; Chipperfield, M., Satellite
490 constraint on the tropospheric ozone radiative effect, *Geophys. Res. Lett.*, 42, 5074-
491 5081, doi: 10.1002/2015GL064037, 2015.
- 492 Riese, M., F. Ploeger, A. Rap, B. Vogel, P. Konopka, M. Dameris, and P. Forster, Impact of
493 uncertainties in atmospheric mixing on simulated UTLS composition and related
494 radiative effects, *J. Geophys. Res.*, 117, D16305, doi: 10.1029/2012JD017751, 2012.
- 495 Roeckner, E., Bauml, G., Bonaventura, L., Brokopf, R., Esch, M., Giorgetta, M., Hagemann,
496 S., Kirchner, I., Kornbluh, L., Manzini, E., Rhodin, A., Schlese, U., Schulzweida, U.,
497 and Tompkins, A.: The atmospheric general circulation model ECHAM5: Part 1, Tech.
498 Rep. 349, Max Planck Institute for Meteorology, Hamburg, 2003.
- 499 Roxy, M. K., Ghosh, S., Pathak, A., Athulya, R., Mujumdar, M., Murtugudde, R., Terray, P.
500 and Rajeevan, M.: A threefold rise in widespread extreme rain events over central
501 India, *Nat. Commun.*, 8(1), 1–11, doi:10.1038/s41467-017-00744-9, 2017.
- 502 Roy, C., Fadnavis, S., Müller, R., Chaudhary, A. D. and Ploeger, F.: Influence of enhanced
503 Asian NO_x emissions on ozone in the Upper Troposphere and Lower Stratosphere
504 (UTLS) in chemistry climate model simulations, *Atmos. Chem. Phys.*, 17, 1297-1311,
505 doi: <https://doi.org/10.5194/acp-17-1297-2017>.
- 506 Santee, M. L., G. L. Manney, N. J. Livesey, M. J. Schwartz, J. L. Neu, and W. G. Read, A
507 comprehensive overview of the climatological composition of the Asian summer
508 monsoon anticyclone based on 10 years of Aura Microwave Limb Sounder
509 measurements, *J. Geophys. Res. Atmos.*, 122, 5491–5514, doi:[10.1002/2016JD026408](https://doi.org/10.1002/2016JD026408),
510 2017.
- 511 Schneider, P. and van Der A, R. J.: A global single-sensor analysis of 2002-2011 tropospheric
512 nitrogen dioxide trends observed from space, *J. Geophys. Res. Atmos.*, 117(16), 1–17,
513 doi: 10.1029/2012JD017571, 2012.
- 514 Stier, P., Feichter, J., Kinne, S., Kloster, S., Vignati, E., Wilson, J., Ganzeveld, L., Tegen, I.,
515 Werner, M., Balkanski, Y., Schulz, M., Boucher, O., Minikin, A. and Petzold, A.: The



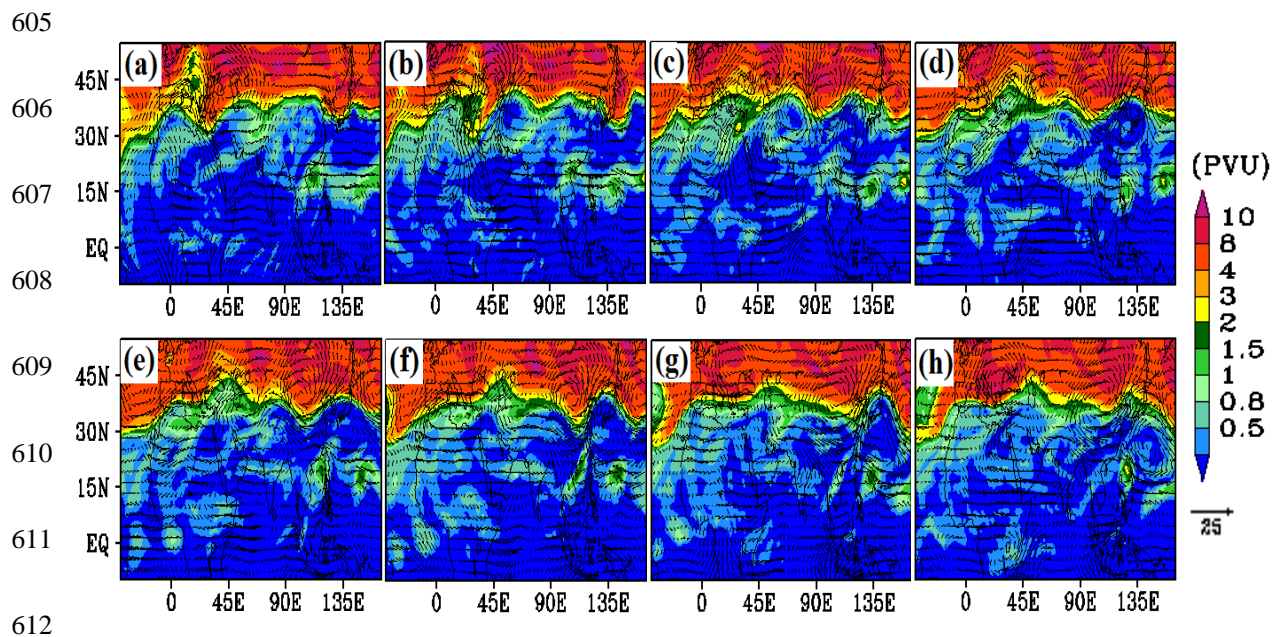
- 516 aerosol-climate model ECHAM5-HAM, Atmos. Chem. Phys., 5, 1125-1156, doi:
517 1680-7324/acp/2005-5-1125, 2005.
- 518 Streets, D. G., Yarber, K. F., Woo, J.-H. and Carmichael, G. R.: Biomass burning in Asia:
519 Annual and seasonal estimates and atmospheric emissions, Global Biogeochem.
520 Cycles, 17(4), doi:10.1029/2003GB002040, 2003.
- 521 Strode, S. A. and Pawson, S.: Detection of carbon monoxide trends in the presence of
522 interannual variability, J. Geophys. Res. Atmos., 118(21), 12257–12273, doi:
523 10.1002/2013JD020258, 2013.
- 524 Strong, C. and Magnusdottir, G.: Tropospheric Rossby Wave Breaking and the NAO/NAM, J.
525 Atmos. Sci., 65(9), 2861–2876, doi:10.1175/2008JAS2632.1, 2008.
- 526 Terezschuk, K. A., Moore, D. P., Harrison, J. J., Boone, C. D., Park, M., Remedios, J. J.,
527 Randel, W. J. and Bernath, P. F.: Observations of peroxyacetyl nitrate (PAN) in the
528 upper troposphere by the Atmospheric Chemistry Experiment-Fourier Transform
529 Spectrometer (ACE-FTS), Atmos. Chem. Phys., 13(11), 5601–5613, doi:10.5194/acp-
530 13-5601-2013, 2013.
- 531 Tie, X., Zhang, R., Brasseur, G. and Lei, W.: Global NO_x Production by Lightning, J. Atmos.
532 Chem., 43(1), 61–74, doi:10.1023/A:1016145719608, 2002.
- 533 Ungermann, J., Ern, M., Kaufmann, M., Müller, R., Spang, R., Ploeger, F., Vogel, B. and
534 Riese, M.: Observations of PAN and its confinement in the Asian summer monsoon
535 anticyclone in high spatial resolution, Atmos. Chem. Phys., 16(13), 8389–8403, doi:
536 10.5194/acp-16-8389-2016, 2016.
- 537 Uppala, S. M., Kållberg, P. W., Simmons, A. J., Andrae, U., da Costa Bechtold, V., Fiorino,
538 M., Gibson, J. K., Haseler, J., Hernandez, A., Kelly, G. A., Li, X., Onogi, K., Saarinen,
539 S., Sokka, N., Allan, R. P., Andersson, E., Arpe, K., Balmaseda, M. A., Beljaars, A. C.
540 M., van de Berg, L., Bidlot, J., Bormann, N., Caires, S., Chevallier, F., Dethof, A.,
541 Dragosavac, M., Fisher, M., Fuentes, M., Hagemann, S., Hólm, E., Hoskins, B. J.,
542 Isaksen, L., Janssen, P. A. E. M., Jenne, R., McNally, A. P., Mahfouf, J. F., Morcrette,
543 J. J., Rayner, N. A., Saunders, R. W., Simon, P., Sterl, A., Trenberth, K. E., Untch, A.,
544 Vasiljevic, D., Viterbo, P. and Woollen, J.: The ERA-40 re-analysis, Q. J. R. Meteorol.
545 Soc., 131(612), 2961–3012, doi:10.1256/qj.04.176, 2005.
- 546 Verstraeten, W. W., Neu, J. L., Williams, J. E., Bowman, K. W., Worden, J. R. and Boersma,
547 K. F.: Rapid increases in tropospheric ozone production and export from China, Nat.
548 Geosci., 8(9), 690–695, doi:10.1038/ngeo2493, 2015.
- 549 Vogel, B., Günther, G., Müller, R., Grooß, J.-U., Hoor, P., Krämer, M., Müller, S., Zahn, A.
550 and Riese, M.: Fast transport from Southeast Asia boundary layer sources to northern
551 Europe: Rapid uplift in typhoons and eastward eddy shedding of the Asian monsoon
552 anticyclone, Atmos. Chem. Phys., 14(23), 12745–12762, doi:10.5194/acp-14-12745-



- 553 2014, 2014.
- 554 Vogel, B., Günther, G., Müller, R., Groß, J.-U., Afchine, A., Bozem, H., Hoor, P., Krämer,
555 M., Müller, S., Riese, M., Rolf, C., Spelten, N., Stiller, G. P., Ungermann, J., and Zahn,
556 A.: Long-range transport pathways of tropospheric source gases originating in Asia
557 into the northern lower stratosphere during the Asian monsoon season 2012, Atmos.
558 Chem. Phys., 16, 15301-15325, <https://doi.org/10.5194/acp-16-15301-2016>, 2016.
- 559 von Clarmann, T., De Clercq, C., Ridolfi, M., Höpfner, M. and Lambert, J. C.: The horizontal
560 resolution of MIPAS, Atmos. Meas. Tech., 2(1), 47–54, doi:10.5194/amt-2-47-2009,
561 2009.
- 562 van der Werf, G. R., Randerson, J. T., Giglio, L., Collatz, G. J., Kasibhatla, P. S. and Arellano,
563 Avelino F., J.: Interannual variability in global biomass burning emissions from 1997
564 to 2004, Atmos. Chem. Phys., 6(11), 3423–3441, doi:10.5194/acpd-6-3175-2006,
565 2006.
- 566 Wang, W.-G., Yuan, M., Wang, H.-Y., Sun, J.-H., Xie, Y.-Q., Fan, W.-X. and Chen, X.-M., A
567 Study of Ozone Amount in the Transition Layer Between Troposphere and
568 Stratosphere and Its Heating Rate. Chinese J. Geophys., 51: 916–930.
569 doi:10.1002/cjg2.1287, 2008
- 570 Wayne, R. P.: Chemistry of the atmospheres, 3rd Edn., Oxford science publications,
571 Clarendon Press, Oxford, 337, 2000.
- 572 Zhang, Q., Wu, G. and Qian, Y.: The Bimodality of the 100 hPa South Asia High and its
573 Relationship to the Climate Anomaly over East Asia in summer. J. Meteorol. Soc.
574 Japan, 80(4), 733–744, doi:10.2151/jmsj.80.733, 2002.
- 575 Zhao, C., Wang, Y., Choi, Y. and Zeng, T.: Summertime impact of convective transport and
576 lightning NO_x production over North America: Modeling dependence on
577 meteorological simulations, Atmos. Chem. Phys., 9(13), 4315–4327, doi: 10.5194/acp-
578 9-4315-2009, 2009.
- 579
- 580
- 581
- 582
- 583
- 584
- 585



586
587
588
589
590
591
592
593
594
595
596
597
598
599
600 Figure 1: Spatial distribution of potential vorticity (PVU) ($1 \text{ PVU} = 10^{-6} \text{ K m}^2 \text{ kg}^{-1} \text{ s}^{-1}$)
601 (color shades) at 370 K potential temperature surface and wind anomalies at 200 hPa
602 from ERA-Interim reanalysis for (a) 01 July, (b) 02 July, (c) 03 July, (d) 04 July, (e) 05 July, (f)
603 06 July, (g) 07 July, (h) 08 July, 2003. Wind vectors are represented by black arrows (m s^{-1}).
604 Eddies are shown with white circles.



613 Figure 2: Spatial distribution of potential vorticity (PVU) (color shades) at 350 K level and
614 wind anomalies in $\text{m}\cdot\text{s}^{-1}$ (thin black vectors) at 200 hPa from ERA-Interim reanalysis for (a)
615 01 July, (b) 02 July, (c) 03 July, (d) 04 July, (e) 05 July, (f) 06 July, (g) 07 July, (h) 08 July,
616 2003. The events of RWB-1, RWB-2 and RWB-3 are indicated by solid black, red and blue
617 arrows, respectively.



618

619

620

621

622

623

624

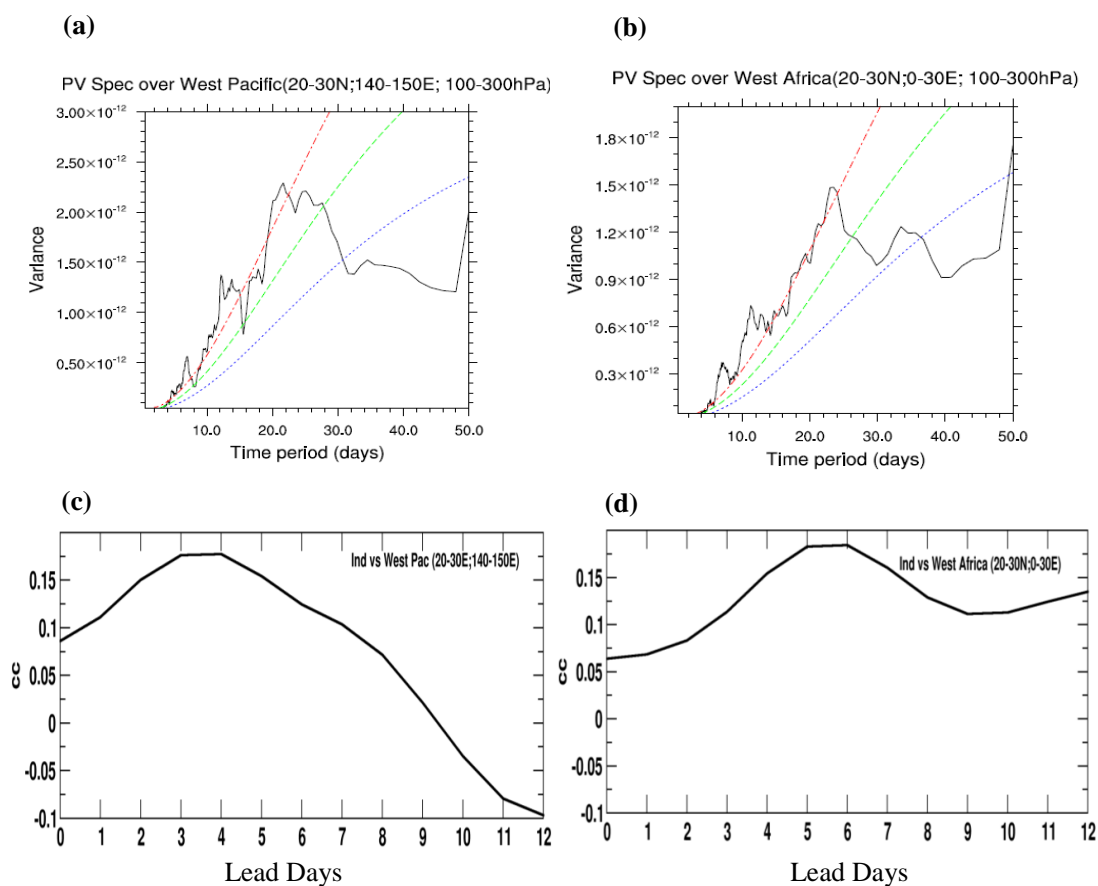
625

626

627

628

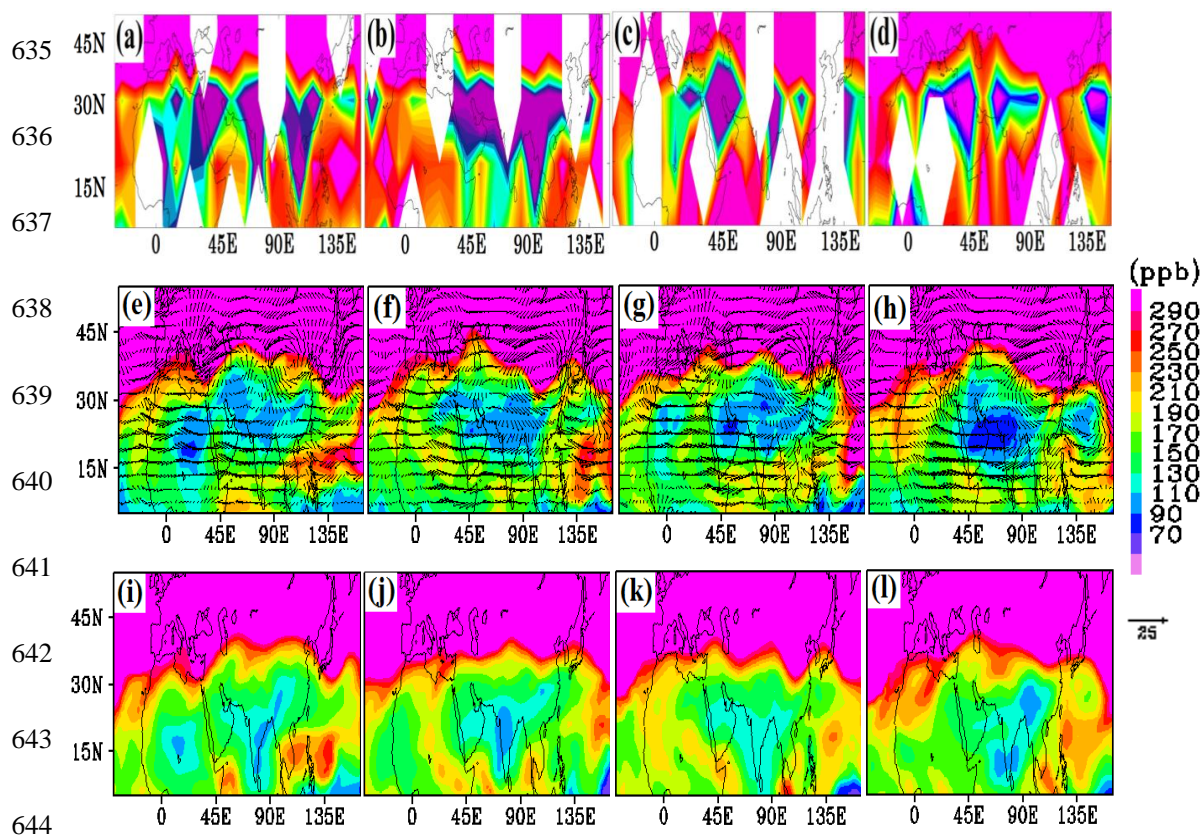
629



630 Figure 3: Power spectral analysis of ERA-Interim PV averaged for 100-300 hPa and in June-
631 September during 1995-2015 (a) West-Africa (20-30° N, 0-30° E) and (b) West-Pacific (20-
632 30° N, 140-150° E) and lag-lead correlation of PV in the monsoon anticyclone (85-90° E, 28-
633 30° N) with (c) West-Pacific (20-30° N, 140-150° E), (d) West Africa (20-30° N, 0-30° E).



634



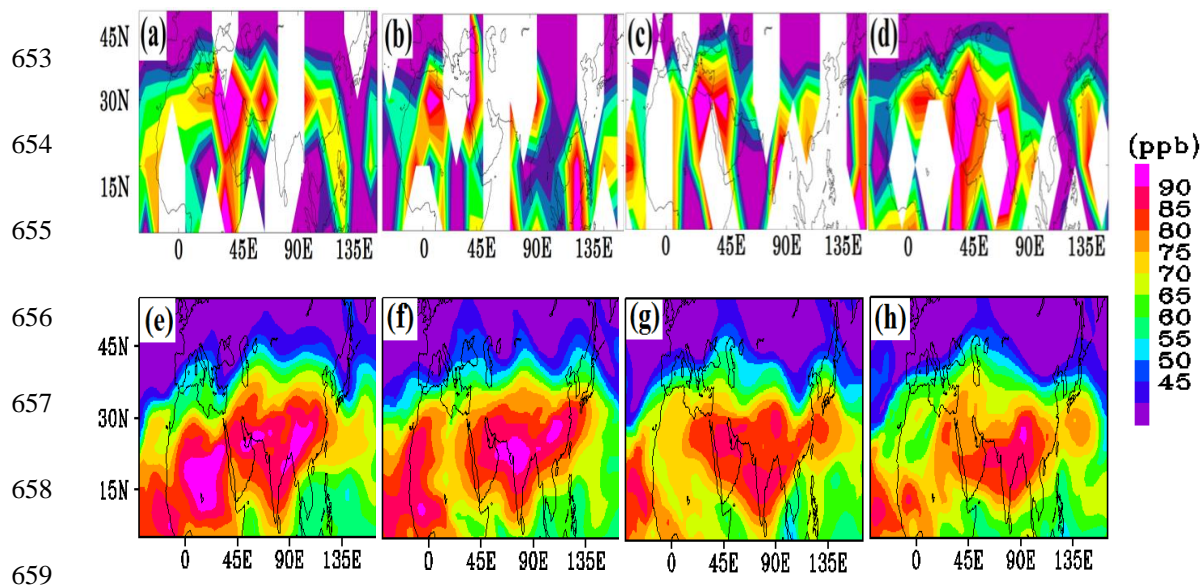
645 Figure 4: Spatial distribution of ozone mixing ratios (ppb) (color shades) corresponding to
646 MIPAS satellite observations at 16 km for (a) 1-2 July, (b) 3-4 July, (c) 5-6 July, (d) 7-8 July,
647 2003; ERA-Interim reanalysis at 100 hPa for (e) 2 July, (f) 4 July, (g) 6 July, (h) 8 July, 2003,
648 and ECHAM5-HAMMOZ CTRL simulations at 16 km for (i) 2 July, (j) 4 July, (k) 6 July, (l) 8
649 July, 2003. Black arrows in panels (e)-(h) show wind anomalies ($\text{m}\cdot\text{s}^{-1}$) at 200 hPa.

650



651

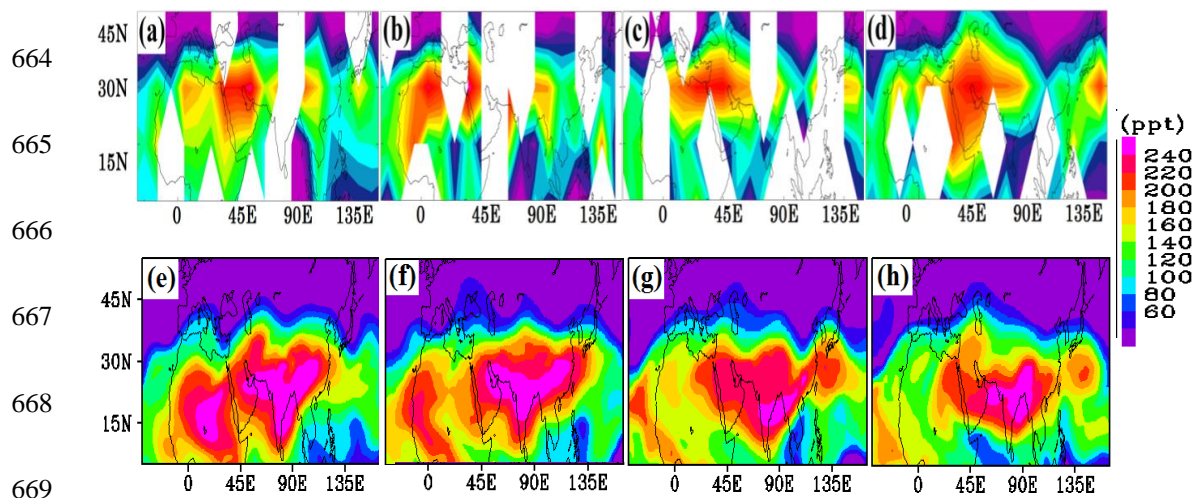
652



660 Figure 5: Spatial distribution of CO mixing ratios (ppb) at 16 km: MIPAS satellite
661 observations for (a) 1-2 July, (b) 3-4 July, (c) 5-6 July, (d) 7-8 July, 2003 and ECHAM5-
662 HAMMOZ CTRL simulations for (e) 02 July, (f) 04 July, (g) 06 July, (h) 08 July, 2003.



663



670 Figure 6: Spatial distribution of PAN mixing ratios (ppt) at 16 km: MIPAS satellite
671 observations for (a) 1-2 July, (b) 3-4 July, (c) 5-6 July, (d) 7-8 July, 2003, and ECHAM5-
672 HAMMOZ CTRL simulations for (e) 02 July, (f) 04 July, (g) 06 July, (h) 08 July, 2003.



673

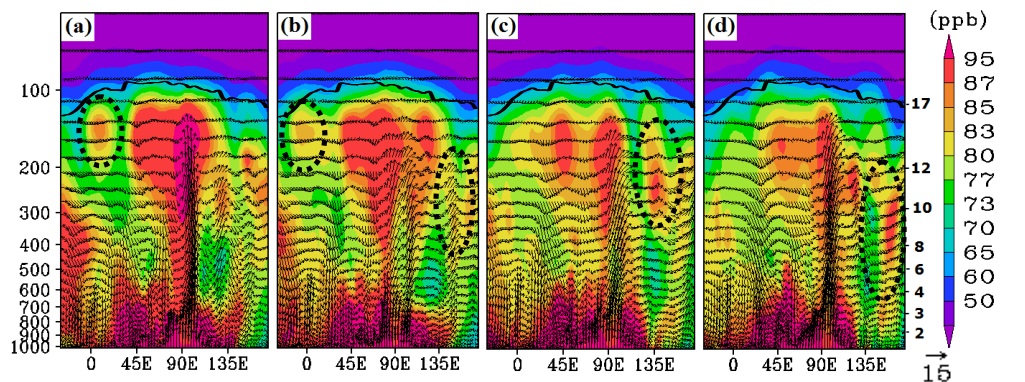
674

675

676

677

678



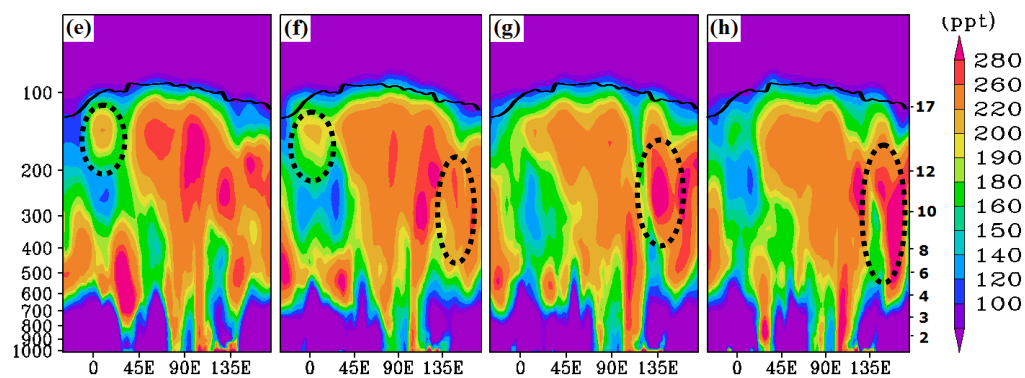
679

680

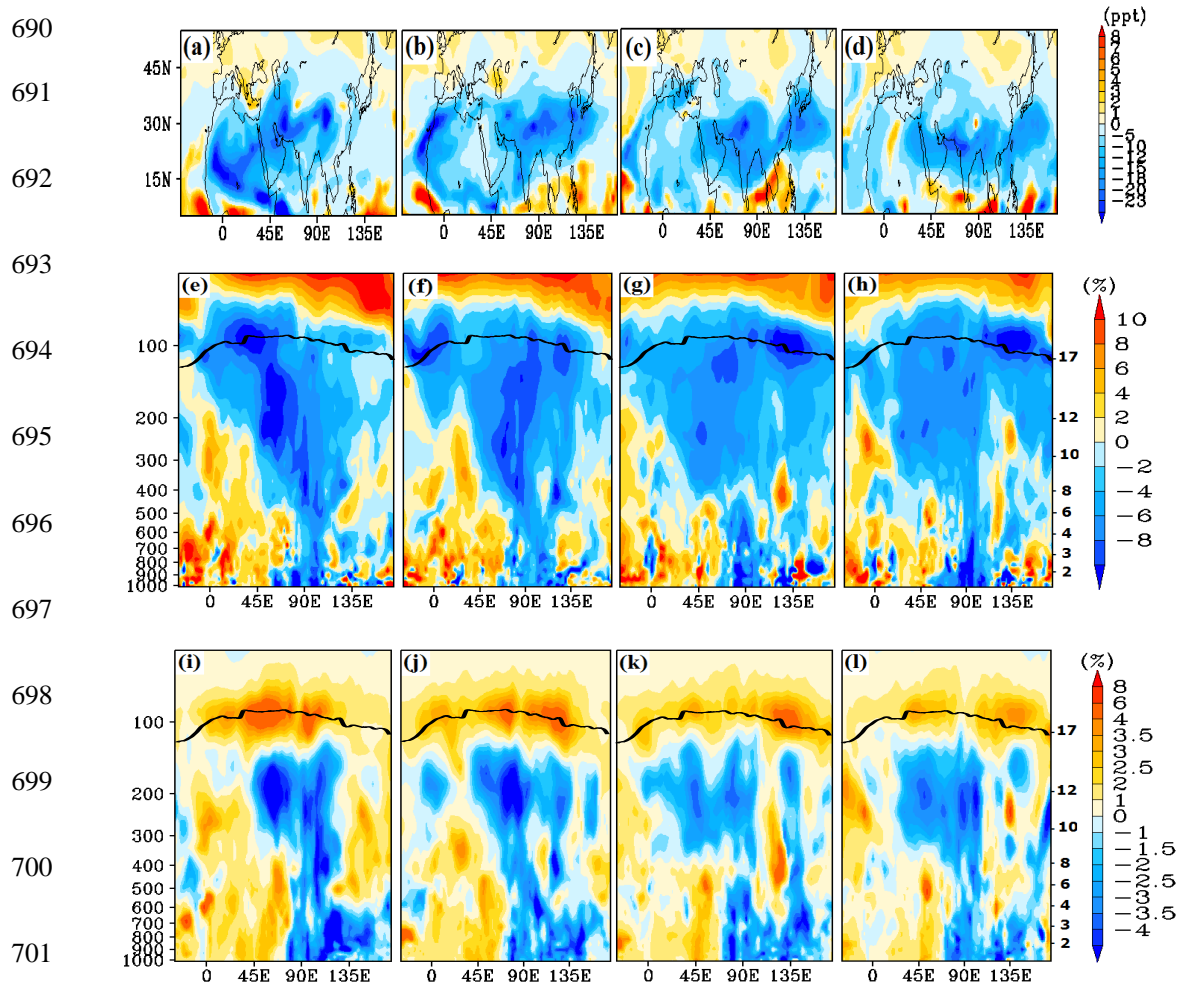
681

682

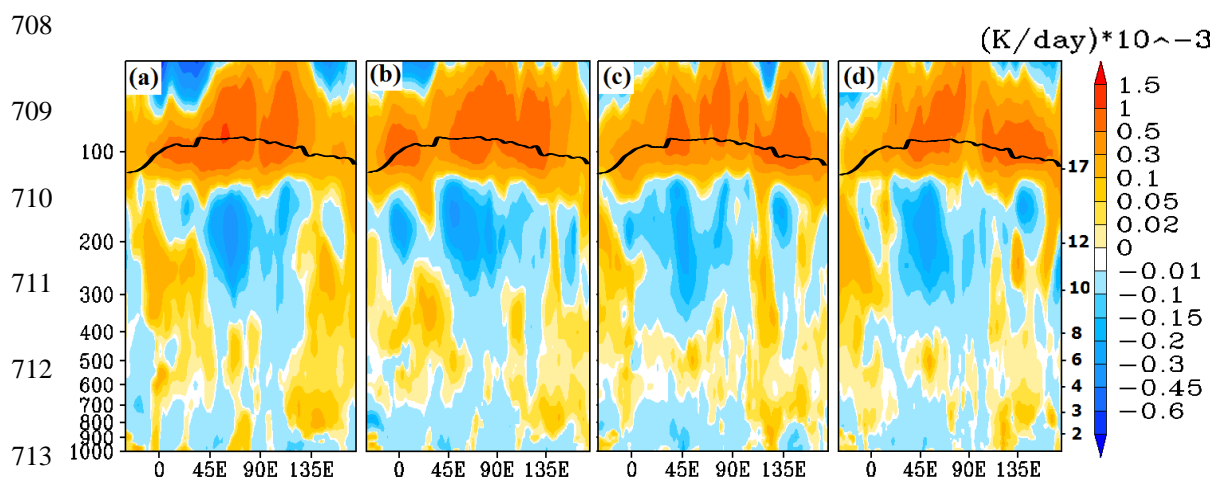
683



684 Figure 7: Longitude-pressure section (averaged for 20°-40° N) of CO (ppb) from
685 ECHAM5-HAMMOZ CTRL simulation for (a) 02 July, (b) 04 July, (c) 06 July, (d) 08 July,
686 2003. Wind vectors ($\text{m}\cdot\text{s}^{-1}$) are shown by black arrows. Vertical velocity field is scaled by a
687 factor of 300. (e)-(h) same as (a)-(d) but for PAN (ppt). Black thick line indicates tropopause and
688 black dotted circles indicate eddies. Pressure (hPa) is indicated on left y-axis and altitudes (km)
689 on right y-axis.



702 Figure 8: Spatial distribution of anomalies of PAN mixing ratios (ppt) (color shades) at 16 km
703 from ECHAM5-HAMMOZ model simulations for (a) 02 July, (b) 04 July, (c) 06 July, (d) 08
704 July, 2003. Longitude-pressure distribution (averaged for 20°-40° N) of anomalies of PAN
705 (%) for (e) 02 July, (f) 04 July, (g) 06 July, (h) 08 July, 2003. (i)-(l) same as (e)-(h) but for
706 ozone anomalies (%). Black thick line indicates tropopause. Pressure (hPa) is indicated on left
707 y-axis and altitudes (km) on right y-axis.



714 Figure 9: Longitude-pressure distribution of anomalies of ozone heating rates ((K·day⁻¹) × 10⁻³)

715 for (a) 02 July, (b) 04 July, (c) 06 July, (d) 08 July, 2003. Pressure (hPa) is indicated on left y-

716 axis and altitudes (km) on right y-axis.

717